

Chaotic Amplification in the Relativistic Restricted Three-body Problem

Lucas F. Wanex

Department of Physics / MS 220 University of Nevada, Reno, Nevada 89557, USA

Reprint requests to Dr. L. W.; Email: lucas@physics.unr.edu, Fax: (775) 784-1398

Z. Naturforsch. **58a**, 13 – 22 (2003); received August 23, 2002

The relativistic equations of motion for the restricted three-body problem are derived in the first post-Newtonian approximation. These equations are integrated numerically for seven different trajectories in the earth-moon orbital system. Four of the trajectories are determined to be chaotic and three are not chaotic. Each post-Newtonian trajectory is compared to its Newtonian counterpart. It is found that the difference between Newtonian and post-Newtonian trajectories for the restricted three-body problem is greater for chaotic trajectories than it is for trajectories that are not chaotic. Finally, the possibility of using this *Chaotic Amplification Effect* as a novel test of general relativity is discussed.

Key words: Relativistic Restricted Three-body Problem; Relativistic Dynamics; Gravitation.

1. Introduction

1.1. A Comparison of General Relativistic and Newtonian Trajectories for the Restricted Three-body Problem

This work uses the *Restricted Three-body Problem* for an analysis of the predictions of the general relativistic equations of motion. The study of the restricted three-body problem has a rich and extended history. The usefulness of studying this problem was verified by the discovery of the Trojan asteroids at the stable Lagrange points of the sun-Jupiter orbital system [1].

The focus of this publication is to study the difference between Newtonian and general relativistic trajectories. The arena for these trajectories is an idealized earth-moon orbital system. Trajectories are calculated numerically using Newtonian and relativistic equations of motion. In order to calculate general relativistic trajectories, the post-Newtonian equations of motion were derived from the Einstein field equations. These equations were derived under the simplifying assumptions of the restricted three-body problem. Seven specific trajectories are presented in section 2. Details of the differences between Newtonian and relativistic examples are presented in section 3.

In the comparisons it is important to note that relativistic and Newtonian trajectories with identical initial conditions were used. Several philosophical and practical objections could be made about this method of

comparison. However, the advice of Michael H. Soffel in his book *Relativity in Astrometry, Celestial Mechanics and Geodesy* was adopted for this work [2]. On page 88 of his book Soffel states, "... one often has to be content with a comparison for equal initial conditions and dynamical parameters."

1.2. The Chaotic Amplification Effect

The method for making these comparisons consists of calculating the Euclidean distance between the final positions as predicted by Newtonian and relativistic trajectories. A consistent feature of these comparisons is that this distance is much larger for chaotic trajectories than it is for non-chaotic trajectories. This feature is the major result obtained in this work and will be called *The Chaotic Amplification Effect*.

2. The Restricted Three-body Problem

2.1. The Definition of the Restricted Three-body Problem

The restricted three-body problem is a special case of the general motion of three bodies moving under the gravitational influences produced by their respective masses. The dynamics of the problem are greatly simplified by considering the situation in which one of the three masses (hereafter called a "*test particle*") is so small that its effect on the motion of the other two

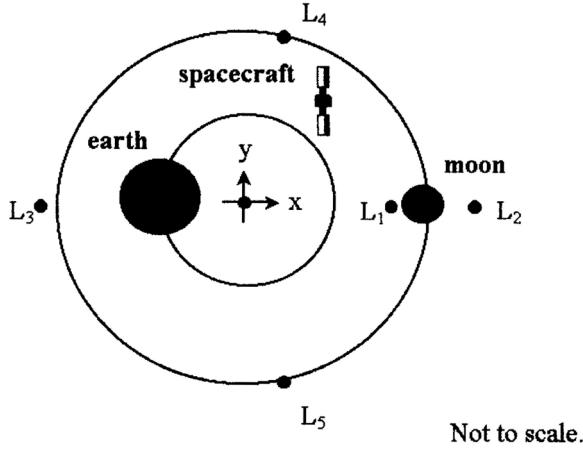


Fig. 1. Two masses such as the earth and moon are considered to be moving on circular paths about their center of mass. The trajectory of a third object, such as a space probe (in the same plane) is calculated numerically. Trajectory calculations are made in a co-rotating frame that has the same angular frequency as the primaries. The points labeled L_1 through L_5 are the “Lagrange Points”.

(hereafter called the “*primaries*”) is negligible. The problem can be further simplified by restricting the motion of the two primary masses (such as the earth and moon) to circular orbits about their center of mass. This circular motion satisfies Newton’s laws if the primaries orbit with the same angular frequency and remain on opposite sides of their center of mass.

The objective of the restricted three-body problem is to calculate the dynamics of the test particle as it moves under the gravitational influence of the primaries. The

results of this paper were obtained with the further simplification that the test particle’s motion is restricted to be in the same plane as the primaries. It is assumed that the mass of the test particle is infinitesimal. By “infinitesimal” it is meant that the mass is so small that it will disturb the motion of the primaries less than the minimum observable distance, during the time under consideration.

For example, the displacement of the earth due to an acceleration caused by the Newtonian gravitational force from an object such as the space shuttle (10^5 kg) at a distance equal to the earth-moon separation is less than 10^{-7} m over a period of three years. The longest time period considered here is about three years, and the smallest displacements considered are on the order of 10^{-4} m.

This work focuses entirely on an idealized system with the primaries having the masses of the earth and moon, and the distance between them equal to the average distance between the actual earth-moon orbital system (these values were obtained from the 2000/2001 CRC [3]).

2.2. Derivation of the Relativistic Equations of Motion

To obtain the relativistic restricted three-body problem equations of motion, the components of the metric tensor were calculated using the post-Newtonian approximation as described by Weinberg [4] (with the exception that they are derived in proper time and not coordinate time). The metric tensor components in a co-rotating frame are

$$\begin{aligned}
 g_{00} &= c^2 - 2 \left(\frac{GM_1}{r_e} + \frac{GM_2}{r_m} \right) + \frac{2}{c^2} \left(\frac{GM_1}{r_e} + \frac{GM_2}{r_m} \right)^2 \\
 &\quad + \frac{2}{c^2} \left(\frac{G^2 M_1 M_2}{r_e (R_1 + R_2)} + \frac{G^2 M_1 M_2}{r_m (R_1 + R_2)} \right) - \left(1 + \frac{2GM_1}{c^2 r_e} + \frac{2GM_2}{c^2 r_m} \right) [\omega^2 (x^2 + y^2)], \\
 g_{01} &= \left(1 + \frac{2GM_1}{c^2 r_e} + \frac{2GM_2}{c^2 r_m} \right) (2\omega y), \\
 g_{02} &= - \left(1 + \frac{2GM_1}{c^2 r_e} + \frac{2GM_2}{c^2 r_m} \right) (2\omega x), \\
 g_{ij} &= - \left(1 + \frac{2GM_1}{c^2 r_e} + \frac{2GM_2}{c^2 r_m} \right) \delta_{ij} \quad (i, j = 1, 2),
 \end{aligned} \tag{1}$$

where r_e and r_m are the distances of the test particle from the earth and moon respectively, R_1 and R_2 are the distances of the earth and moon from the cen-

ter of mass, and M_1 , M_2 are the masses of the earth and moon. With this metric tensor one obtains the Lagrangian [5]

$$L = \frac{1}{2} g_{ij} \frac{dx^i}{d\tau} \frac{dx^j}{d\tau}, \quad x^0 = t, x^1 = x, x^2 = y \quad (2)$$

for the Euler-Lagrange equations

$$\frac{d}{d\tau} \left(\frac{\partial L}{\partial \dot{x}^i} \right) - \frac{\partial L}{\partial x^i} = 0, \quad (3)$$

where a dot means the derivative with respect to proper time τ . The equations of motion (in proper time, i.e., for an observer on the test particle) obtained by this method are as follows:

$$\begin{aligned} \ddot{x} = & 2\omega\dot{y}\dot{t} + \omega^2 x \dot{t}^2 + \omega y \ddot{t} - G \left(\frac{M_1(x+R_1)}{r_e^3} + \frac{M_2(x-R_2)}{r_m^3} \right) \dot{t}^2 \\ & + \frac{2G}{c^2} \left\{ \begin{aligned} & \left(\frac{M_1[(x+R_1)\dot{x} + y\dot{y}]}{r_e^3} + \frac{M_2[(x-R_2)\dot{x} + y\dot{y}]}{r_m^3} \right) (\dot{x} - \omega y \dot{t}) \\ & + \left(\frac{M_1}{r_e} + \frac{M_2}{r_m} \right) (-\ddot{x} + 2\omega\dot{y}\dot{t} + \omega y \ddot{t} + \omega^2 x \dot{t}^2) \\ & + G \left[\begin{aligned} & \left(\frac{M_1}{r_e} + \frac{M_2}{r_m} \right) \left(\frac{M_1(x+R_1)}{r_e^3} + \frac{M_2(x-R_2)}{r_m^3} \right) \\ & + \frac{M_1 M_2}{2(R_1+R_2)} \left(\frac{1}{r_e^3} + \frac{1}{r_m^3} \right) \end{aligned} \right] \dot{t}^2, \\ & - \left(\frac{M_1(x+R_1)}{2r_e^3} + \frac{M_2(x-R_2)}{2r_m^3} \right) (U^2 + \omega^2 R^2 \dot{t}^2 + 2\omega i A) \end{aligned} \right\}, \quad (4) \end{aligned}$$

$$\begin{aligned} \ddot{y} = & -2\omega\dot{x}\dot{t} + \omega^2 y \dot{t}^2 - \omega x \ddot{t} - G \left(\frac{M_1}{r_e^3} + \frac{M_2}{r_m^3} \right) y \dot{t}^2 \\ & + \frac{2G}{c^2} \left\{ \begin{aligned} & \left(\frac{M_1[(x+R_1)\dot{x} + y\dot{y}]}{r_e^3} + \frac{M_2[(x-R_2)\dot{x} + y\dot{y}]}{r_m^3} \right) (y + \omega x \dot{t}) \\ & + \left(\frac{M_1}{r_e} + \frac{M_2}{r_m} \right) (-\ddot{y} - 2\omega\dot{x}\dot{t} - \omega x \ddot{t} + \omega^2 y \dot{t}^2) \\ & + G \left[\begin{aligned} & \left(\frac{M_1}{r_e} + \frac{M_2}{r_m} \right) \left(\frac{M_1}{r_e^3} + \frac{M_2}{r_m^3} \right) \\ & + \frac{M_1 M_2}{2(R_1+R_2)} \left(\frac{1}{r_e^3} + \frac{1}{r_m^3} \right) \end{aligned} \right] y \dot{t}^2 \\ & - y \left(\frac{M_1}{2r_e^3} + \frac{M_2}{2r_m^3} \right) (U^2 + \omega^2 R^2 \dot{t}^2 + 2\omega i A) \end{aligned} \right\}, \quad (5) \end{aligned}$$

$$\dot{t} = \frac{K + A\omega}{c^2} + \frac{K \left(\frac{2GM_1}{r_e} + \frac{2GM_2}{r_m} + \omega^2 R^2 \right)}{c^4}, \quad (6)$$

where t represents the coordinate time, K is a constant of motion, and

$$U^2 = \dot{x}^2 + \dot{y}^2,$$

$$A = \dot{y}x - \dot{x}y, \quad (7)$$

$$R^2 = x^2 + y^2.$$

The angular frequency ω of the rotating frame has the value obtained for the relativistic two-body problem [6]. The constant of motion arises because the coordinate time does not appear explicitly in the

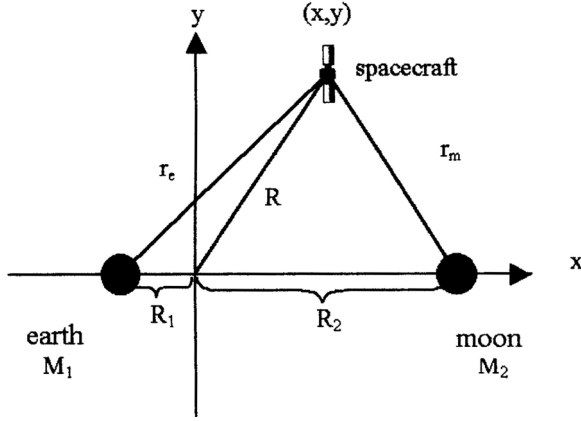


Fig. 2. The definitions of the symbols in the equations of motion can be seen here.

Lagrangian. This constant can be obtained from the initial conditions and is $\cong c^2$. These equations are accurate to $O(1/c^2)$. The definitions of the symbols in the equations of motion can be seen in Figure 2.

2.3. Testing the Correctness of the Equations of Motion

The equations of motion were numerically integrated using the Gear polynomial extrapolation method [7]. Discreteness parameters were tested to assure that results do not depend on the numerical approximation accuracy. Thirty two bit words, a relative error per step of 10^{-14} and a minimum step size of 10^{-11} sec were sufficient for this purpose.

Because of the complexity involved in obtaining the general relativistic equations of motion their correctness was rigorously tested. Four different kinds of tests were performed.

1. The equations in the Newtonian limit.
2. Limiting cases.
3. Constancy of the constant of motion K .
4. Reversal tests to check the accuracy of the software used.

Test 1. The equations of motion in the Newtonian limit

If the equations of motion are correct they should be identical to the equations of motion of the Newtonian restricted three-body problem when they are extrapolated to the Newtonian limit ($c \rightarrow \infty$). It is easily

shown that under this limit these equations match exactly with the equations for the Newtonian restricted three-body problem as given by Moulton [8] and Szebehely [9].

Test 2. Limiting cases

If the equations of motion are correct they should reproduce expected results when solved numerically. For example, if the mass of either of the primaries is set to zero, the motion should correspond to that of the relativistic case in which an infinitesimally small test particle orbits about a massive primary. General relativistic predictions say that under these conditions the test particle should exhibit an advance of the line of apsides. This is identical to the perihelion advance of Mercury in its orbit about the sun [10]. Excellent agreement between the numerical value and the theoretical value [11] for this test was obtained.

Test 3. The constant of motion

Because the relativistic restricted three-body problem Lagrangian does not involve the coordinate time explicitly the Euler-Lagrange equations show that

$$\frac{d}{dt} \left(\frac{\partial L}{\partial \dot{t}} \right) = 0 \Rightarrow \frac{\partial L}{\partial \dot{t}} = K, \quad (8)$$

where L is the Lagrangian, \dot{t} is the derivative of the coordinate time with respect to the proper time τ , and K is a constant. The value of this constant can be determined from the initial position and velocity of the test particle. Comparing the value of K obtained from the initial conditions to the value of K obtained from the final position and velocity of a numerical integration of the equations of motion allows for a sensitive test of the results obtained. This test was performed on all the results presented here with a typical relative error of $\sim 0.2 \times 10^{-27}$.

Test 4. Reversal tests

The accuracy of numerical integrations was checked using reversal tests. This is done by specifying an initial position and velocity and integrating the equations of motion forward in time. The final position and velocity of this numerical integration are then used as the initial conditions of a second numerical integration. This second computer run integrates the equations of motion backwards in time. The final position and velocity of this numerical integration should be the same

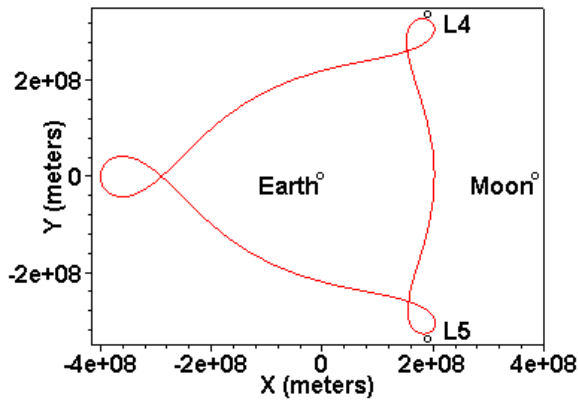


Fig. 3. Rosette orbit.

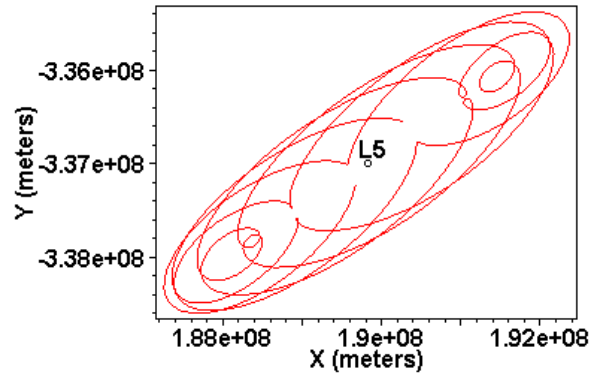


Fig. 5. Tadpole trajectory near L_5 .

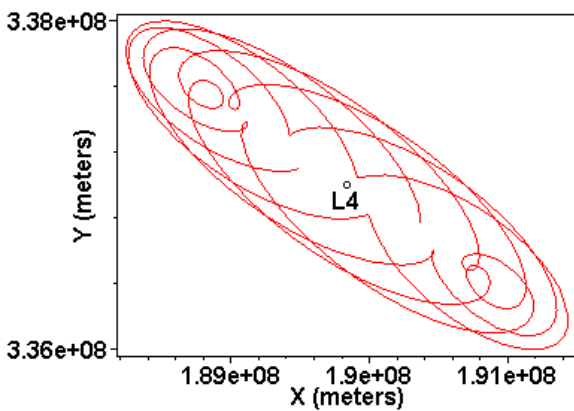


Fig. 4. Tadpole trajectory near L_4 .

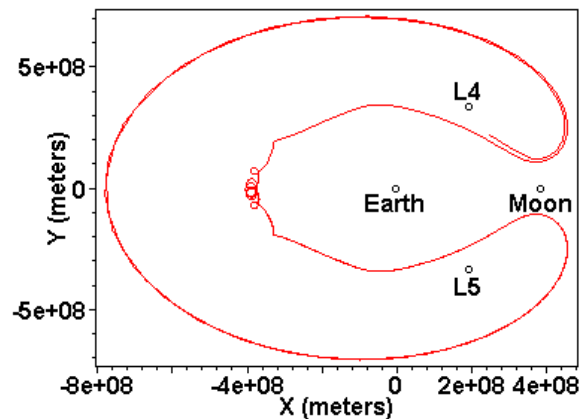


Fig. 6. Earth-Moon Horseshoe trajectory.

as the initial position and velocity of the first numerical integration. In order to integrate backwards in time the final velocity of the first integration has the same magnitude but is reversed. Also, the negative of the angular frequency of the primaries must be used.

Typical relative errors for the results presented here were $\sim 10^{-12}$ resulting in an accuracy in position on the order of 10^{-4} m. These small error values give a high degree of confidence in the correctness of the numerical integration method used.

2.4. Trajectory Examples

Seven trajectories will be used to illustrate the Chaotic Amplification Effect. Four of these are chaotic and the other three are not chaotic.

The tadpole trajectories depicted in Figs. 4 and 5 are stable because the test particle remains in the vicinity of L_4 and L_5 infinitely [12]. The rosette orbit in Fig. 3

closes on itself and repeats infinitely, so it is also stable. The trajectories depicted in Figs. 6–9 are all chaotic. Table 1 lists the initial positions and velocities for all trajectories presented here.

2.5. Chaos in the General Relativistic Restricted Three-body Problem

The chaotic nature of the relativistic earth-moon horseshoe trajectory is illustrated by comparing Figures 10 and 11. These two plots show the path of two nearby trajectories over a period of 16 months. The initial conditions for these two trajectories differ by only 1 cm in position on the x -axis. The test particle begins to depart on opposite sides of the horseshoe shaped path. The difference between the final positions of the two is 4311 m after 14 months. This indicates that the relativistic earth-moon horseshoe trajectory is chaotic in the sense that a small change in the initial condi-

Table 1. Trajectory Initial Conditions.

Fig.	Name	x-position	y-position	x-velocity	y-velocity
3	Rosette orbit	$-3.9976409920664 \cdot 10^8$ m	0 m	0 m/s	210.0 m/s
4	Tadpole trajectory near L_4	$1.895 \cdot 10^8$	$3.371 \cdot 10^8$	-0.111	0
5	Tadpole trajectory near L_5	$1.897 \cdot 10^8$	$-3.372 \cdot 10^8$	-0.179	0
6	Horseshoe trajectory	$3.749610003 \cdot 10^8$	0	0	-84.81
7	Exchange trajectory	$4.38 \cdot 10^8$	0	0	32.8
8	Near Earth	$1.921872312 \cdot 10^6$	0	0	10912.0
9	Lunar Encounter	$-4.0215520053 \cdot 10^8$	0	0	166.85

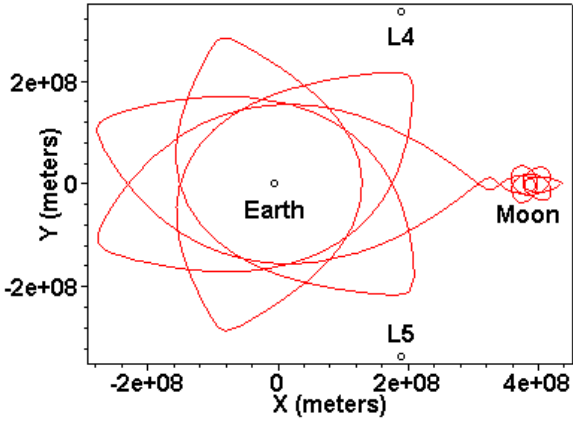


Fig. 7. Earth-Moon Exchange trajectory.

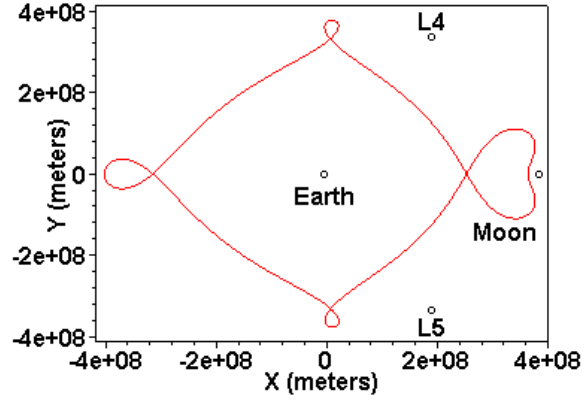


Fig. 9. Lunar Encounter trajectory.

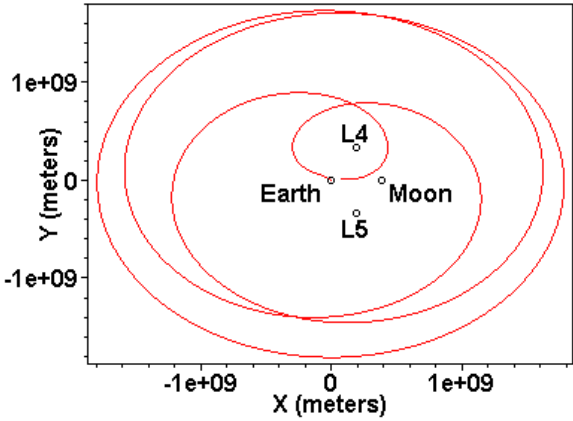


Fig. 8. Near Earth trajectory.

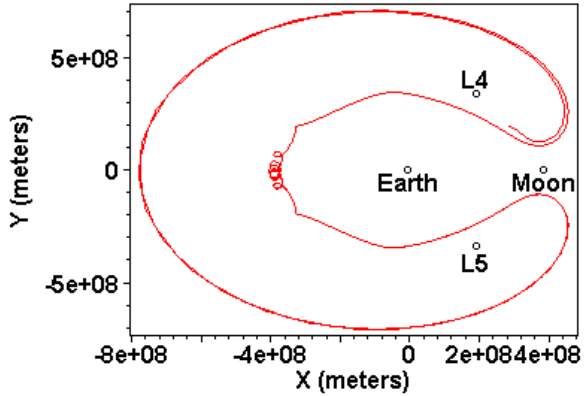


Fig. 10. The final position is inside the horseshoe shaped path.

tions results in a relatively large difference 14 months later.

Chaos is characterized by an exponentially growing distance between nearby trajectories [13]. Chaotic trajectories in the Newtonian restricted three-body problem should also be chaotic in the relativistic three-body problem [14]. It would be difficult to assume that a trajectory that is chaotic with the Newtonian equa-

tions could become a trajectory that is not chaotic with the post-Newtonian equations since the relativistic corrections are small and the post-Newtonian equations reduce to the Newtonian equations in the Newtonian limit. With this in mind the chaotic nature of each of the above trajectories was determined using the Newtonian equations of motion [15]. Table 2 lists the re-

Table 2. Newtonian Chaos Analysis.

Trajectory	Chaotic Behavior	Approximate Lyapunov Exponents
Horseshoe	chaotic	0.044/day (from 12 – 25 months)
Exchange	chaotic	0.019/day (from 8 – 30 months)
Near Earth	chaotic	0.042/day (from 4 – 16 months)
Lunar Encounter	chaotic	0.014/day (from 4 – 10 months)
Rosette	not chaotic	NA
L_4 Tadpole	not chaotic	NA
L_5 Tadpole	not chaotic	NA

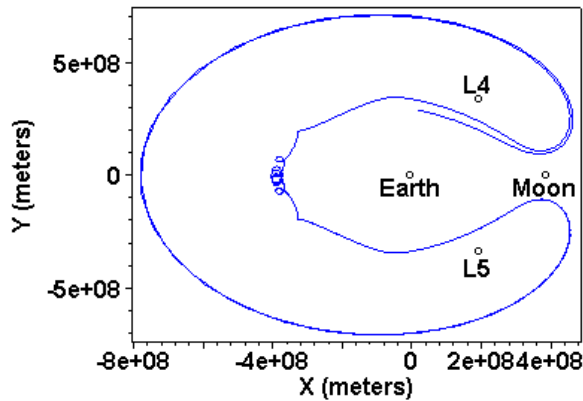


Fig. 11. The final position is outside the horseshoe shaped path.

sults of this analysis. Figures 12 and 13 explain the information presented in Table 2.

The linear nature of the plot in Fig. 12 from approximately 12 months to 25 months indicates that the average growth in distance between the horseshoe trajectory and nearby trajectories is exponential in character. This indicates that the horseshoe trajectory is chaotic. The Lyapunov exponent was estimated by averaging the slope of the lines between 12 and 25 months for each of the 100 test trajectories.

Figure 13 indicates that there is no sustained period of exponential growth in distance between nearby trajectories for the rosette orbit. This orbit is not chaotic over the time period considered here.

3. Comparing Newtonian and Relativistic Trajectories

3.1. Numerical Results for the Difference between Newtonian and Relativistic Trajectories

A comparison of the difference between general relativistic and Newtonian trajectories with identical initial conditions illustrates the Chaotic Amplification Ef-

Table 3. Differences in final positions for Newtonian and relativistic trajectories after 14 months.

Trajectory	Euclidean Distance (meters)
Horseshoe	$2.6 \cdot 10^2$
Exchange	$3.1 \cdot 10^4$
Near Earth	$2.7 \cdot 10^8$
Lunar Encounter	$2.5 \cdot 10^9$
Rosette	$3.5 \cdot 10^{-1}$
L_4 Tadpole	$5.5 \cdot 10^{-1}$
L_5 Tadpole	$7.3 \cdot 10^{-1}$

fect. The difference between Newtonian and general relativistic motion after 14 months is much larger for the four chaotic trajectories than it is for the three trajectories that are not chaotic.

3.2. The Chaotic Amplification Effect

The distances between the test particle's final positions as listed in Table 3 reveal a remarkable result. The difference is much larger for the chaotic trajectories. The relatively large differences in final positions for the chaotic trajectories are surprising because relativistic corrections are typically on the order of the Schwarzschild radius $2GM/c^2$, which in this case is ~ 1 cm per orbit. In the light of these results it is apparent that chaos amplifies the difference between Newtonian and relativistic trajectories.

The cause of this amplification can be understood by considering the earth-moon horseshoe trajectory in an inertial frame (Figure 14). This trajectory consists of ten rotations of the test particle about the earth-moon center of mass. Consider the situation after one circuit of the test particle about the center of mass. The final position of this trajectory as predicted by Newtonian and relativistic integrations will differ by at least 1 cm. Now consider a new calculation in which these are the initial conditions of two new trajectories. One of these corresponds to the Newtonian prediction while the other corresponds to the relativistic prediction. The Newtonian part of the relativistic equations will cause similar chaotic motion for both predictions. A difference of 1 cm in the initial conditions results in a period of exponentially increasing distance between nearby trajectories (as shown in Figure 12). So it is seen that chaos amplifies the difference between Newtonian and relativistic trajectories.

3.3. Time Evolution of the Chaotic Amplification

The difference between Newtonian and relativistic trajectories grows rapidly over time for chaotic

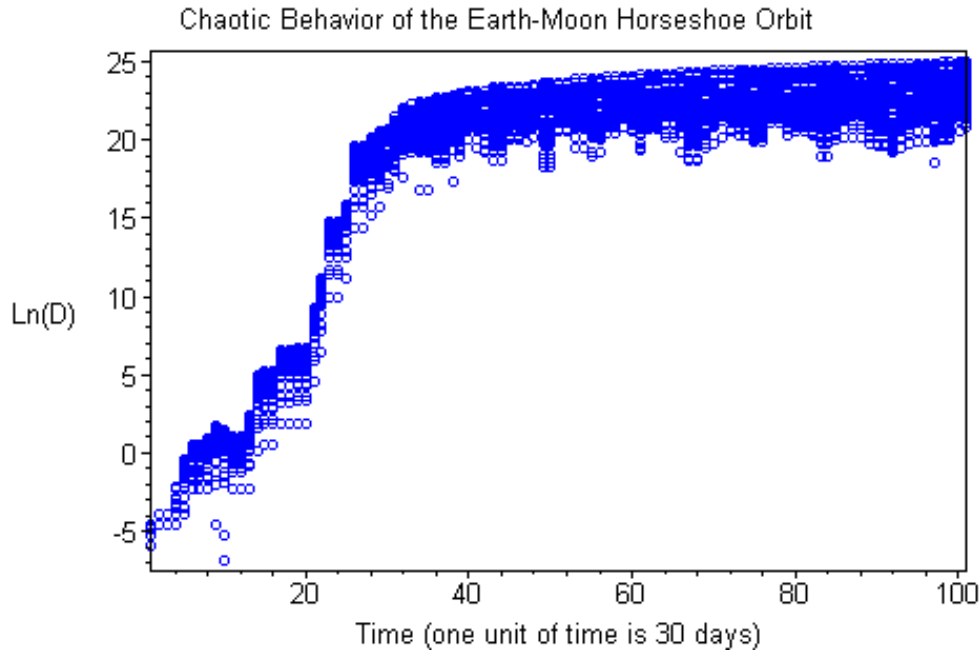


Fig. 12. This is a plot of the log of the distance between a test particle in the horseshoe trajectory and one in 100 nearby trajectories.

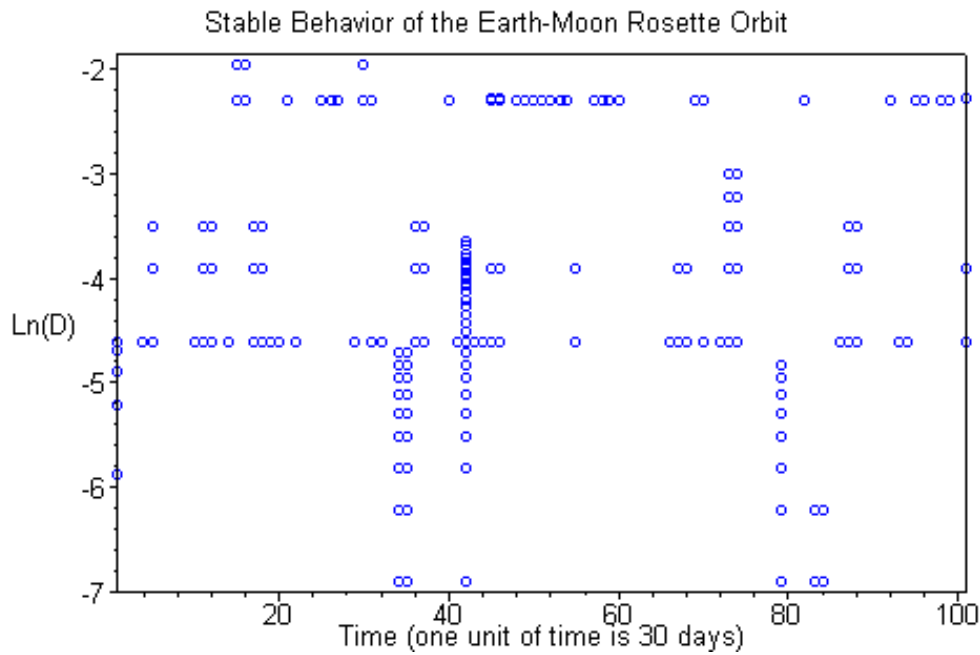


Fig. 13. This is a plot of the log of the distance between a test particle in the rosette orbit and one in 100 nearby orbits.

trajectories. The earth-moon horseshoe trajectory clearly illustrates this effect. The distance between the two cases becomes very large within a period of 3 years.

The distance between a test particle in the Newtonian and relativistic earth-moon horseshoe trajectory versus time is illustrated in Figure 15. As can be seen the distance begins to grow rapidly after 25 months.

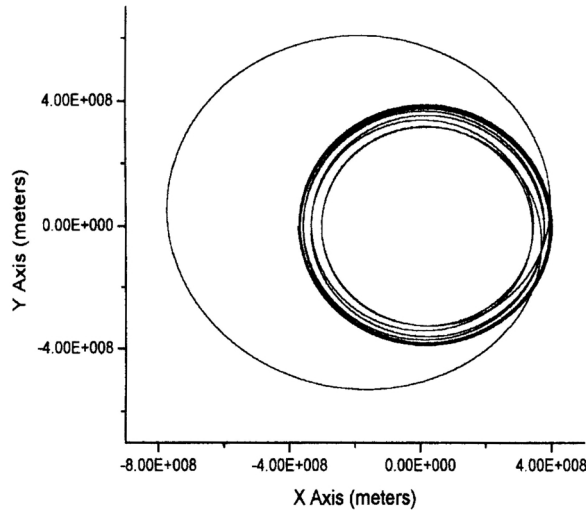


Fig. 14. The earth-moon horseshoe trajectory in an inertial frame.

After approximately 33 months the distance is more than 10 times the earth-moon separation, which is approximately 4×10^8 m. In order for this large separation to occur some type of gravity assist, in which the test particle gains energy from the earth or moon must take place. This gravity assist phenomena was used by NASA to propel the voyager spacecraft from the solar system. In 1972 M. A. Minovitch published a general theorem about this effect [16].

For example, the test particle can gain kinetic energy as it passes the moon. Initially the test particle will gain energy as it approaches the moon, and then it will lose energy as it moves away from the moon. The test particle approaches and departs from the vicinity of the moon with the same velocity relative to the moon. However, it picks up the velocity of the moon in its orbit about the center of mass of the earth-moon orbital system. The energy gained can propel the test particle to large distances from the earth-moon center of mass.

4. Conclusion

The existence of the Trojan asteroids confirms the usefulness of predicting natural phenomena in the solar system using the restricted three-body problem. This makes it reasonable to assume that the chaotic amplification effect exists in the earth-moon orbital system. Perturbations from the other planets in the solar system will not eliminate the chaotic amplification effect even if they are larger than the results presented here. This can be seen by considering the perihelion advance

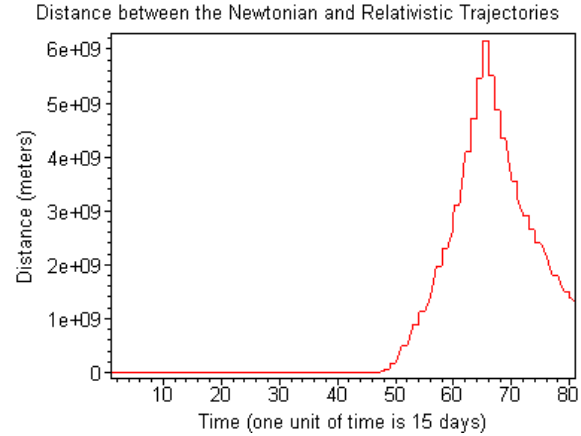


Fig. 15. Distance between Newtonian and relativistic trajectories versus time for the earth-moon horseshoe trajectory.

of Mercury. The actual observed advance is 574 arcseconds per century. After the perturbations due to the other planets in the solar system are subtracted out, 43 arcseconds per century remains as predicted by general relativity [17]. This shows that solar system perturbations do not cancel the relatively small perihelion advance. Similarly, once the planetary perturbations are subtracted out, the chaotic amplification effect should still be present.

The existence of the chaotic amplification effect suggests the possibility of using this phenomenon to perform a novel test of Einstein's theory of gravity. A space probe could be placed in a chaotic trajectory and tracked. A comparison of the tracking data with the predictions of general relativity could, in principle, be done. As shown above, planetary perturbations will not cancel the chaotic amplification. Perturbations from solar wind, radiation pressure, cosmic rays, etc. can be eliminated using drag free technology. Such drag-free technology [18] is already being developed for other space missions such as Gravity Probe B [19], STEP [20], and LISA [21].

However, the practical aspects of performing such a test are quite formidable. Chaos is characterized by extreme sensitivity to initial conditions. Any errors in the initial position and velocity of the space probe result in large unknowns later in time. These uncertainties are as large as or larger than the effects of chaotic amplification.

Today's laser ranging facilities can determine the position of a space probe in the earth-moon orbital system to an accuracy of ~ 1 cm [22]. To overcome the

sensitivity to initial conditions inherent in chaotic trajectories the position of a satellite must be known to better than 10^{-4} meters for the earth-moon horseshoe trajectory. This makes it necessary for the test to await a great improvement in our current technological abilities.

Acknowledgement

I am indebted to Professor F. Winterberg for suggesting the relativistic restricted three-body problem as an area of research and his continued guidance

and support for this project. Recognition also goes to Donovan Haxton and Tom Bryant of the Goddard Space Flight Center for writing initial versions of software that assisted in locating the Newtonian earth-moon horseshoe trajectory. Acknowledgement for optimizing the computer code used for integrating the restricted three-body problem's Newtonian and relativistic equations of motion should also be given to Allan Wittkopf of Waterloo Maple, Inc. I would also like to thank Greggory Stefanelli (University of Nevada Computer Systems Administrator) for providing access to the Hercules computer in the University's library.

- [1] G. Abell, *Exploration of the Universe*, Holt, Rinehart and Winston, New York 1974, p. 341.
- [2] M. H. Soffel, *Relativity in Astrometry, Celestial Mechanics and Geodesy*, Springer-Verlag, Berlin 1989 p. 88.
- [3] *CRC Handbook of Chemistry and Physics*, Editor-in-Chief David R. Lide, CRC Press, New York 2000–2001.
- [4] S. Weinberg, *Gravitation and Cosmology Principles and Applications of the General Theory of Relativity*, John Wiley & Sons, New York 1972, Chapt. 9.
- [5] J. Foster, J. D. Nightingale, *A Short Course in General Relativity*, Springer, New York 1995, p. 62.
- [6] M. H. Soffel, *Relativity in Astrometry, Celestial Mechanics and Geodesy*, Springer-Verlag, Berlin 1989, p. 173.
- [7] C. W. Gear, *Numerical Initial Value Problems in Ordinary Differential Equations*, Prentice-Hall, Englewood Cliffs, New Jersey 1971, Chapt. 6.
- [8] F. R. Moulton, *An Introduction To Celestial Mechanics*, Dover Publications, New York 1970, p. 153.
- [9] V. Szebehely, *Theory of Orbits*, Academic Press, New York 1967, p. 21.
- [10] C. M. Will, *Was Einstein Right?*, BasicBooks, New York 1986, Chapt. 5.
- [11] J. Foster and J. D. Nightingale, *A Short Course in General Relativity*, Springer, New York 1995, p. 147.
- [12] F. R. Moulton, *An Introduction to Celestial Mechanics*, Dover Publications, New York 1970, p. 298.
- [13] G. J. Sussman, J. Wisdom, *Science* **241**, 433 (1988).
- [14] S. Rosswog, D. Trautmann, *Planet. Space Sci.* **44**, No. 4, 313 (1996).
- [15] L. F. Wanex, *Chaotic Amplification in the Relativistic Restricted Three-Body Problem*, Ph.D. Dissertation, University of Nevada, Reno, 26 (2002).
- [16] M. A. Minovitch, *Journal of Spacecraft and Rockets* **9**, 751 (1972).
- [17] C. M. Will, *Was Einstein Right?*, BasicBooks, New York 1986, p. 91.
- [18] L. Vaillon, J. Borde, T. Duhamel, P. Damilano, *Space Technol.* **16**, No. 5/6, 245 (1996).
- [19] B. Lange, *Phys. Rev. D* **59**, 102004-1 (1999).
- [20] R. Reinhard, Y. Jafry, R. Laurance, *ESA Journal* **17**, 251 (1993).
- [21] J. W. Cornelisse, *Class. Quantum Grav.* **13**, A251 (1996).
- [22] G. Bianco, M. Chersich, R. Devoti, V. Luceri, and M. Selden, *Geophysical Research Letters* **28**, 2113 (2001).